

Probing a light CP-odd scalar in di-top-associated production at the LHC

Mirkoantonio Casolino,¹ Trisha Farooque,¹ Aurelio Juste,^{1,2} Tao Liu,³ and Michael Spannowsky⁴¹*Institut de Física d'Altes Energies (IFAE), E-08193 Bellaterra, Barcelona, Spain*²*Institució Catalana de Recerca i Estudis Avançats (ICREA), E-08010 Barcelona, Spain*³*Department of Physics, The Hong Kong University of Science and Technology, Clear Water Bay, Kowloon, Hong Kong S.A.R., P.R.C.*⁴*Institute for Particle Physics Phenomenology, Department of Physics, Durham University, DH1 3LE, United Kingdom*

CP-odd scalars are an integral part of many extensions of the Standard Model. Recently, electroweak-scale pseudoscalars have received increased attention in explaining the diffuse gamma-ray excess from the Galactic Centre. Elusive due to absence of direct couplings to gauge bosons, these particles receive only weak constraints from direct searches at LEP or searches performed during the first LHC runs. We investigate the LHC's sensitivity in observing a CP-odd scalar in di-top associated production in the mass range $20 \leq m_A \leq 100$ GeV using jet substructure based reconstruction techniques. We parametrise the scalar's interactions using a simplified model approach and relate the obtained upper limits on couplings within type-I and type-II 2HDMs as well as the NMSSM. We find that in di-top-associated production, experiments at the LHC can set tight limits on CP-odd scalars that fit the Galactic Centre excess. However, direct sensitivity to light CP-odd scalars from the NMSSM proves to remain challenging.

I. INTRODUCTION

The recent discovery of the Higgs boson [1, 2] marked a new era for fundamental physics. For the first time an electroweak-scale scalar resonance has been discovered, supposedly a remnant of the mechanism underlying electroweak symmetry breaking [3].

While elementary scalar particles have been observed in nature for the first time, they are often an integral part of Standard Model (SM) extensions, e.g. Supersymmetry or general N-Higgs Doublet Models. When these extensions contain complex scalar fields, as a result, CP-odd scalars are introduced to the spectrum of the theory. Hence, since their existence would be evidence for physics beyond the SM, searches for CP-odd scalars are at the core of the current LHC program.

Recently, CP-odd scalars as mediators between Dark Matter (DM) and SM particles have received attention in explaining the diffuse gamma-ray excess from the Galactic Centre [4–7] in the contexts of the so-called Coy Dark Matter models [8–10], and the Next-to-Minimal-Supersymmetric-Standard-Model (NMSSM) [11, 12]. Hence, they are included as mediators in simplified models by the ATLAS and CMS collaborations to recast searches for jets and missing transverse energy ('monojet') during the upcoming LHC runs [13, 14].

In contrast to the widely accepted paradigm that new physics particles have to be heavy, i.e. masses of $\mathcal{O}(1)$ TeV or beyond, the mass of CP-odd scalars is almost unconstrained by direct searches. As interactions between gauge bosons and CP-odd scalars are only induced via higher-dimensional operators, e.g. $\frac{1}{2}A\epsilon_{\mu\nu\sigma\rho}V_{\sigma\rho}V^{\mu\nu}$, limits from LEP are fairly weak. The main collider sensitivities may mainly arise from bottom quark or top quark-associated productions (for recent explorations, see [15, 16]). Further, due to the predicted velocity suppression in direct detection experiments for CP-odd scalar mediators, even light CP-odd scalars are still in agreement with experimental observations. Some constraints from flavour physics exist but limits are again weak if $m_A \gtrsim 5$ GeV [17], assuming the CP-odd scalar interacts with fermions in agreement with the hypothesis of minimal flavour violation [18].

Therefore, indirect detection experiments and direct searches at the LHC appear to be the most sensitive ways to search for the existence of electroweak-scale CP-odd scalar particles. In this paper, instead of previously explored paths of searching for CP-odd scalars in gluon-fusion production [19, 20], we focus on the direct production of such particles in association with a top quark pair and subsequent decay into a bottom quark pair, $pp \rightarrow t\bar{t}A \rightarrow t\bar{t}b\bar{b}$. Thus, we derive limits on the mass and coupling strength of the CP-odd scalar in a process with unsuppressed fermion couplings only.¹

This paper is organised as follows. In Sec. II we briefly outline the way we incorporate the CP-odd scalar into the theory, using a simplified model approach. The event generation and details of the final state reconstruction are

¹ We note that, if the pseudoscalar couples for example in a universal way to fermions as part of a UV-complete model, thereby not respecting Yukawa-like coupling hierarchies, other production and decay channels might be more sensitive. However, the analysis we provide is still valid as a subset of possible search channels.

described in detail in Secs. III and IV. In Sec. V we derive limits on the mass of the CP-odd scalar and its couplings to top quarks. Such limits can be applied to models where the CP-odd scalar arises as part of a Higgs multiplet. We recast these limits in the context of the 2HDM and the NMSSM in Sec. VI. Finally, in Sec. VII we offer conclusions.

II. SIMPLIFIED MODEL

While CP-odd scalars are present in many extensions of the SM, for simplicity and generality of our results, we use a simplified model approach [21] to parametrise the contribution of this particle in the process $pp \rightarrow t\bar{t}A \rightarrow t\bar{t}b\bar{b}$. More precisely, we add couplings of the CP-odd scalar with the bottom and top quarks to the full SM Lagrangian

$$\mathcal{L} = \mathcal{L}_{\text{SM}} + \mathcal{L}_{\text{CP-odd}}, \quad (1)$$

where

$$\mathcal{L}_{\text{CP-odd}} = i\frac{g_t y_t}{\sqrt{2}} \bar{t}\gamma_5 t A + i\frac{g_b y_b}{\sqrt{2}} \bar{b}\gamma_5 b A, \quad (2)$$

and g_i ($i = t, b$) parametrises the deviation from the SM Yukawa coupling $y_i = m_i/v$.

Recently, a similar approach was proposed to recast monojet searches at the LHC in terms of scalar mediators between the SM and a secluded sector [22–25]. In a similar way, we will focus on the minimal set of free parameters relevant to the process considered. Throughout this paper we will assume A to be a narrow resonance with $2m_b \leq m_A < 2m_t$. Hence, in our approach the CP-odd scalar decays exclusively into bottom quarks with $\mathcal{B}(A \rightarrow b\bar{b}) = 1$ and its width Γ_A is completely determined by the value of g_b . For a narrow resonance, the kinematic distributions are expected to remain largely independent of the value of Γ_A .

III. EVENT GENERATION AND SIMULATION DETAILS

A. Signal and background modelling

Signal and background samples corresponding to pp collisions at $\sqrt{s} = 14$ TeV are generated using the MADGRAPH5 2.1.1 [26] leading-order (LO) generator and the CTEQ6L1 [27] set of parton distribution functions (PDF), interfaced to PYTHIA v6.427 [28] for parton showering and fragmentation and using the Perugia2011C [29] underlying event tune. In all cases, a top quark mass of 172 GeV is assumed and top quarks are decayed inclusively by PYTHIA.

Samples of $t\bar{t}A$ signal events are generated for different values of the A boson mass, $m_A = 20, 30, 40, 60, 80$ and 100 GeV, and assuming $g_t = 1$ and $\mathcal{B}(A \rightarrow b\bar{b}) = 1$. A model corresponding to the Lagrangian shown in Eq. 1 is implemented using Feynrules 2.1 [30] and imported as UFO model [31] in MADGRAPH5. The LO signal cross section predicted by MADGRAPH5 (see Table I) is scaled by a k-factor of 1.3. This k-factor is obtained as the ratio of the NLO to LO cross sections for $t\bar{t}h$ production, where h is a CP-even Higgs boson. It has been checked that this k-factor is rather constant as a function of m_h , varied between 20 and 125 GeV. Figure 1(a) compares the production cross section between $t\bar{t}h$ and $t\bar{t}A$ as a function of the Higgs boson mass, in both cases assuming $g_t=1$. The ratio between both cross sections varies significantly versus mass, with the $t\bar{t}h$ cross section being about a factor of 20 larger than the $t\bar{t}A$ cross section at a mass of 20 GeV, and only about a factor of two larger at a mass of 120 GeV [32]. This difference results from the presence of the extra γ_5 factor in the interaction between a CP-odd Higgs boson and the top quark, compared to the case of a CP-even Higgs boson. Another consequence of the different interaction is that a CP-odd Higgs boson has a substantially harder p_T spectrum compared to the CP-even case, particularly at low mass, as illustrated in Fig. 1(b). This is a key feature exploited in this analysis, as discussed in Sec. IV.

m_A (GeV)	20	30	40	60	80	100
$\sigma^{\text{LO}}(t\bar{t}A)$ (pb)	0.46	0.42	0.39	0.32	0.27	0.23

TABLE I: Leading-order cross section for $t\bar{t}A$ production in pp collisions at $\sqrt{s} = 14$ TeV as a function of the A boson mass m_A . As discussed in the text, this LO cross section is obtained assuming $g_t = 1$ and will be multiplied by a k-factor of 1.3 to approximate the NLO cross section.

A large sample of $t\bar{t}$ +jets background events is generated with up to two additional partons in the 5F scheme (i.e. including b - and c -quarks). To avoid double-counting of partonic configurations generated by both the matrix-element

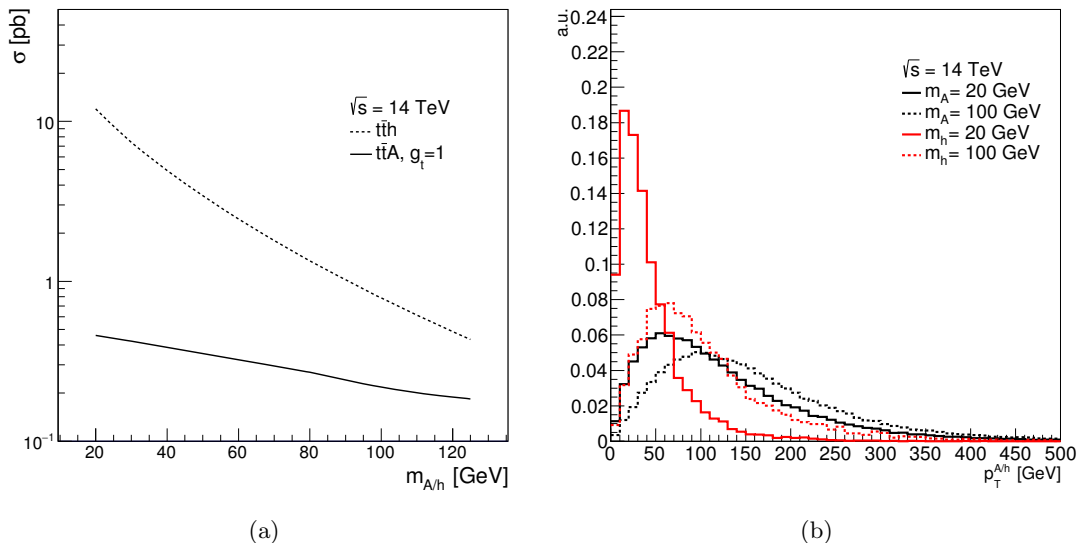


FIG. 1: (a) Comparison of the leading-order cross section for $t\bar{t}h$ (solid line) and $t\bar{t}A$ (dashed line) in pp collisions at $\sqrt{s} = 14$ TeV as a function of Higgs boson mass. In both cases a value of $g_t = 1$ is assumed. (b) Comparison of the Higgs boson p_T between $t\bar{t}h$ (red) and $t\bar{t}A$ (black) for two different values of the Higgs boson mass, 20 GeV (solid) and 100 GeV (dashed).

calculation and the parton shower, a parton-jet matching scheme (“MLM matching”) [33] is employed. The sample is normalised to a cross section of 990 pb obtained using TOP++ v2.0 [34] at next-to-next-to-leading order (NNLO) in QCD, including resummation of next-to-next-to-leading logarithmic (NNLL) soft gluon terms [35–39], and using the MSTW 2008 NNLO [40, 41] PDF set. The $t\bar{t}$ +jets sample is generated inclusively, but events are categorised depending on the flavour content of additional particle jets in the event (i.e. jets not originating from the decay of the $t\bar{t}$ system). Particle jets are reconstructed with the anti- k_t [42–44] algorithm with a radius parameter $R = 0.4$ and are required to have $p_T > 15$ GeV and $|\eta| < 2.5$. Events where at least one such particle jet is matched within $\Delta R < 0.4$ to a b -hadron with $p_T > 5$ GeV not originating from a top quark decay are generically labelled as $t\bar{t}+\geq 1b$ events. Similarly, events where at least one such particle jet is matched within $\Delta R < 0.4$ to a c -hadron with $p_T > 5$ GeV not originating from a W boson decay, and that are not labelled already as $t\bar{t}+\geq 1b$, are labelled as $t\bar{t}+\geq 1c$ events. Events labelled as either $t\bar{t}+\geq 1b$ or $t\bar{t}+\geq 1c$ are generically referred to below as $t\bar{t}$ +HF events, where HF stands for “heavy flavour”. We do not apply dedicated corrections to the normalisation of $t\bar{t}$ +HF events, since Run 1 searches at the LHC [45] showed that the LO prediction from MADGRAPH5 using the same settings as us is consistent with data within $\sim 20\%$, and a larger systematic uncertainty will be assumed in this study. As in Ref. [45], a finer categorisation of $t\bar{t}$ +HF events is considered for the purpose of assigning systematic uncertainties associated with the modelling of heavy-flavour production in different topologies. In this way, a distinction is made between events with only one extra heavy-flavour jet satisfying the above cuts (referred to as $t\bar{t}+b$ or $t\bar{t}+c$), events with two extra heavy-flavour jets (referred to as $t\bar{t}+b\bar{b}$ or $t\bar{t}+c\bar{c}$), and events with one extra heavy-flavour jet containing two b - or c -hadrons (referred to as $t\bar{t}+B$ or $t\bar{t}+C$). The remaining events are labelled as $t\bar{t}$ +light-jet events, including those with no additional jets.

Additional background samples corresponding to $t\bar{t}W$, $t\bar{t}Z$ and $t\bar{t}h_{\text{SM}}$ production, where h_{SM} is the SM Higgs boson, are also produced. The $t\bar{t}W$ sample is generated requiring at least one W boson in the event to decay leptonically, and is normalised to the corresponding LO cross section, 0.404 pb, times a k-factor of 1.4 [46]. The $t\bar{t}Z$ sample is generated requiring $Z \rightarrow q\bar{q}$ decays and is normalised to the corresponding LO cross section, 0.353 pb, times a k-factor of 1.3 [46]. Finally, the $t\bar{t}h_{\text{SM}}$ sample is generated assuming $m_h = 125$ GeV and requiring $h \rightarrow b\bar{b}$ decays. It is normalised to the NLO cross section [47–49], 0.611 pb, times the $h_{\text{SM}} \rightarrow b\bar{b}$ branching ratio of 57.7% [50–53], collected in Ref. [54]. In these samples $Z \rightarrow q\bar{q}$ and $h_{\text{SM}} \rightarrow b\bar{b}$ decays are performed by MADGRAPH5 and top quarks and W bosons are decayed by PYTHIA.

B. Event reconstruction

The generated samples at the particle level are processed through a simplified simulation of the detector response and object reconstruction.

Isolated leptons (electrons or muons) are required to originate from a W boson or τ -lepton decay and to have $p_T > 25$ GeV and $|\eta| < 2.5$. Furthermore, they are required to not overlap with jets, as discussed below. A typical per-lepton identification efficiency of 80% is assumed.

Stable particles from PYTHIA, except for muons and neutrinos, are processed through a simplified simulation of a calorimeter. The four momenta of particles falling within the same window in η - ϕ space of size $\Delta\eta \times \Delta\phi = 0.1 \times 0.1$ are added together to simulate the finite granularity of calorimeter cells. For each cell, the total three momentum is rescaled such as to make the cell massless. Cells with energy larger than 0.1 GeV and $|\eta| < 5.0$ become the inputs to the jet algorithm. Several types of jets are considered in this analysis.

The anti- k_t algorithm is used to reconstruct jets with two different radius parameters, $R = 0.2$ and $R = 0.4$, referred to as AKT2 and AKT4 jets respectively. The minimum jet p_T threshold for reconstruction is 5 GeV. During jet reconstruction, no distinction is made between identified electrons and jet energy deposits, and so every electron is also reconstructed a jet. In order to remove this double counting, if any of the jets in the AKT2 and AKT4 collections lie within $\Delta R = 0.2$ of a selected electron, the closest jet from each jet collection is discarded. Since this analysis has a large number of b -quark initiated jets, for which a significant fraction of energy is carried away by muons in semi-muonic b -hadron decays, the four momenta of all reconstructed muons with $p_T > 4$ GeV that are ghost-associated [55, 56] to a jet are added to the calorimeter jet four momentum. After this correction, a minimum p_T requirement of 15 GeV and 25 GeV is made for AKT2 and AKT4 jets respectively. All jets are required to satisfy $|\eta| < 2.5$. Finally, any electron or muon within $\Delta R = 0.4$ of a selected AKT4 jet is discarded. In this analysis AKT4 jets are used to define the minimum jet multiplicity required in the event selection, while AKT2 jets are used to define the b -tag multiplicity of the event. The latter is particularly important since at low m_A values the b -quarks from the $A \rightarrow b\bar{b}$ decay emerge with small angular separation. The flavour of an AKT2 jet is determined by matching it within $\Delta R = 0.15$ with a b -hadron or a c -hadron (not originating from a b -hadron decay), resulting in the jet being labelled as b -jet or c -jet respectively. The rest of the jets are taken to originate from the fragmentation of a light quark or gluon and are labelled as “light jets”. Heavy-flavour tagging is modelled in a probabilistic fashion by assigning a per-jet efficiency of 70% to b -jets, 20% to c -jets, and 0.7% to light jets.

In addition, jets are reconstructed with the Cambridge-Aachen (C/A) algorithm [57, 58] in order to reconstruct the $A \rightarrow b\bar{b}$ decay, taking advantage of the boost with which A bosons are produced in the $t\bar{t}A$ process. Two radius parameters are considered for C/A jets, $R^{C/A} = 0.6$ and 0.8, referred to as CA6 and CA8 jets respectively. The choice of radius for C/A jets is optimised in order to optimally reconstruct the $t\bar{t}A$ signal depending on the value of m_A . In order to minimise the impact of soft radiation and pileup (not modelled in this analysis), the mass-drop (a.k.a. BDRS) filtering algorithm [59, 60] with the following parameters, $\mu_{\text{frac}} = 0.67$ and $y_{\text{cut}} = 0.09$ [61], is applied to the reconstructed C/A jets. A semi-muonic energy correction to the C/A jet four momentum is also applied, as in the case of AKT2 and AKT4 jets.

IV. EXPERIMENTAL ANALYSIS

A. Analysis strategy and event selection

This search is focused on the $t\bar{t}A \rightarrow W^+bW^-b\bar{b}$ process, with one of the W bosons decaying leptonically and the other W boson decaying hadronically. Only electrons or muons originating from W boson or τ -lepton decays are considered. The resulting final state signature is thus characterised by one electron or muon, and high jet and b -jet multiplicity that can be exploited to suppress the background, dominated by $t\bar{t}$ +jets production. Therefore, the following preselection requirements are made: one electron or muon, ≥ 5 AKT4 jets and ≥ 3 AKT2 b -tagged jets, in the following simply referred to as ≥ 5 jets and ≥ 3 b -tags. In order to optimise the sensitivity of the search, the selected events are categorised into two separate channels depending on the number of b -tags (3 and ≥ 4). The channel with ≥ 5 jets and ≥ 4 b -tags has the largest signal-to-background ratio and therefore drives the sensitivity of the search. It is dominated by $t\bar{t}$ +HF background. The channel with 3 b -tags has significantly lower signal-to-background ratio and the background is enriched in $t\bar{t}$ +light-jets. The simultaneous analysis of both channels is particularly useful to calibrate *in-situ* the $t\bar{t}$ +jets background prediction (including its heavy-flavour content) and constrain the related systematic uncertainties, as it will be discussed in Sec. IV C. This is a common strategy used in many experimental searches in the ATLAS and CMS collaborations [45, 62, 63], which we mimic here in order to obtain more realistic projected sensitivities.

An extra handle is provided by the significant boost of the A boson in a fraction of signal events, which results in the two b -jets from the $A \rightarrow b\bar{b}$ decay emerging with small angular separation between them. This is particularly relevant for low m_A values, as shown in Fig. 2. As a result, the A boson decay products can be reconstructed into a single fat jet, whose mass distribution would show a resonant structure peaked at the correct m_A value. This feature is also very powerful to discriminate against the background. Therefore, a further requirement is made to have at

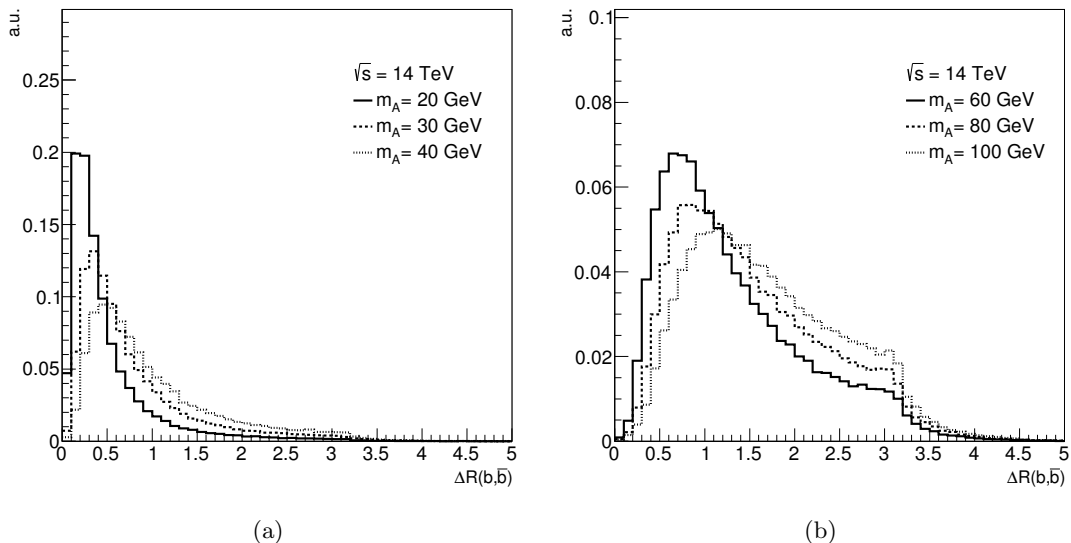


FIG. 2: Distribution of ΔR between the two b -quarks from the $A \rightarrow b\bar{b}$ decay prior to any selection requirements, for different values of m_A : (a) $m_A = 20, 30$ and 40 GeV, and (b) $m_A = 60, 80$ and 100 GeV.

least one C/A BDRS-filtered jet with radius parameter R^{CA} and minimum p_T depending on the m_A hypothesis being tested. In order to correctly reconstruct a significant fraction of the signal while rejecting as much background as possible, CA6 jets are used for $m_A \leq 40$ GeV, while CA8 jets are used for higher m_A values (up to 100 GeV). The minimum p_T requirements on the C/A jets are 60, 100, 120, 150, 200 and 250 GeV for $m_A = 20, 30, 40, 60, 80$ and 100 GeV, respectively. As shown in Fig. 2, for high values of m_A only a small fraction of signal events would have the A decay products contained within the CA8 jet. The small signal acceptance comes with the benefit of improved background rejection and the ability to reconstruct the A boson mass, desirable in such simple analysis. However, it is expected that a dedicated multivariate analysis focused on the sample rejected by this analysis, similar in spirit to the ATLAS and CMS searches for the SM Higgs boson in $t\bar{t}h$, $h \rightarrow b\bar{b}$ [45, 62], could also achieve significant signal sensitivity at high m_A . Evaluating this possibility is beyond the scope of this study. The number of b -tags inside the C/A jet is determined by matching the b -tagged AKT2 jets within a cone of radius $\Delta R = 0.75R^{C/A}$. Finally, a requirement is made is that the C/A jets have ≥ 2 b -tags inside. In case of more than one selected C/A jet, the leading p_T one is chosen.

Table II presents the expected yields for signal and the SM backgrounds per fb^{-1} of integrated luminosity as a function of the selection cuts applied in each of the analysis channels under consideration: $(\geq 5j, 3b)$ and $(\geq 5j, \geq 4b)$. In the case of the $(\geq 5j, 3b)$ channel, the dominant background after final selection is $t\bar{t}$ +light-jets, where typically the two b -quarks from the top quark decays, as well as the c -quark from the $W \rightarrow c\bar{s}$ decay, are b -tagged. In contrast, in the $(\geq 5j, \geq 4b)$ channel half of the background is $t\bar{t}+\geq 1b$, with $t\bar{t}+b\bar{b}$ being its leading contribution. The rest of the background is approximately equally split between $t\bar{t}+\geq 1c$ and $t\bar{t}$ +light-jets. In this table the expected contribution from $t\bar{t}A$ signal is obtained under the assumptions of $g_t = 2$ and $\mathcal{B}(A \rightarrow b\bar{b}) = 1$. Both analysis channels have approximately the same amount of signal, while the background is about a factor of four higher in the $(\geq 5j, 3b)$ channel than in the $(\geq 5j, \geq 4b)$ channel. Together with the different composition of the background, the very different signal-to-background ratio between both channels is the primary motivation for analysing them separately.

The final discriminating variable is the invariant mass of the selected C/A jet, referred to as “leading BDRS jet mass”. Figures 3 and 4 show the expected distribution of the BDRS jet mass for signal and background in each of the analysis channels, for the different m_A values considered. The distributions correspond to $\sqrt{s} = 14$ TeV and are normalised to an integrated luminosity of 30 fb^{-1} . For the assumed values of $g_t = 2$ and $\mathcal{B}(A \rightarrow b\bar{b}) = 1$, the signal is clearly visible on top of the background.

B. Systematic uncertainties

Several sources of systematic uncertainty are considered that can affect the normalisation of signal and background and/or the shape of the BDRS jet mass distribution. Individual sources of systematic uncertainty are considered

	$t\bar{t}+\geq 1b$	$t\bar{t}+\geq 1c$	$t\bar{t}+\text{light-jets}$	$t\bar{t}+X$	Total bkg.	$t\bar{t}A$
$m_A = 30 \text{ GeV}$						
1 lepton	4167	10958	155648	299	171072	377
≥ 5 jets	3109	7678	61866	215	72868	268
3 b -tags	766	765	2702	30.1	4263	72.4
≥ 1 CA6 jets	510	502	1485	21.4	2518	55.7
≥ 2 b -tags in selected CA6 jet	45.1	38.4	159	1.9	245	14.6
≥ 4 b -tags	234	100	128	10.6	474	28.7
≥ 1 CA6 jets	171	70.1	75.7	7.9	325	23.8
≥ 2 b -tags in selected CA6 jet	36.9	13.2	18.5	1.5	70.2	11.7
$m_A = 80 \text{ GeV}$						
1 lepton	4167	10958	155648	299	171072	240
≥ 5 jets	3109	7678	61866	215	72868	198
3 b -tags	766	765	2702	30.1	4263	57.5
≥ 1 CA8 jets	252	246	646	11.5	1155	23.6
≥ 2 b -tags in selected CA8 jet	32.3	32.8	125	2.0	192	6.1
≥ 4 b -tags	234	100	128	10.6	474	25.0
≥ 1 CA8 jets	91.6	36.4	35.0	4.3	167	11.6
≥ 2 b -tags in selected CA8 jet	25.8	10.6	12.6	1.5	50.4	5.3

TABLE II: Expected signal and SM backgrounds at $\sqrt{s} = 14 \text{ TeV}$ per fb^{-1} of integrated luminosity as a function of the selection cuts applied in each of the analysis channels under consideration (see text for details): ($\geq 5j$, 3b) and ($\geq 5j$, $\geq 4b$). The signal prediction is obtained under the assumptions of $g_t = 2$ and $\mathcal{B}(A \rightarrow b\bar{b}) = 1$. Several background categories have been merged for readability. The sum of $t\bar{t}+W$, $t\bar{t}+Z$ and $t\bar{t}+h_{\text{SM}}$ is denoted as $t\bar{t}+X$. The yields shown correspond to the optimised selections for two different values of m_A , 30 GeV and 80 GeV. Shown in bold are the signal and backgrounds expectations after full selection in each of the analysis channels considered.

uncorrelated. Correlations of a given systematic uncertainty are maintained across processes and analysis channels. The choices of what uncertainties to consider and their magnitude are inspired by recent $t\bar{t}+h_{\text{SM}}$, $h_{\text{SM}} \rightarrow b\bar{b}$ searches at the LHC [45].

A 15% normalisation uncertainty is assigned to $t\bar{t}+\text{light-jets}$ corresponding to the modelling of the jet multiplicity spectrum. A 30% normalisation uncertainty is assigned to each of the $t\bar{t}+\text{HF}$ components ($t\bar{t}+b$, $t\bar{t}+b\bar{b}$, $t\bar{t}+B$, $t\bar{t}+c$, $t\bar{t}+c\bar{c}$, $t\bar{t}+C$), and taken to be uncorrelated among them. These uncertainties are expected to be conservative given the recent progress in NLO predictions for $t\bar{t}$ with up to two jets merged with a parton shower [64], as well as NLO predictions for $t\bar{t}+\geq 1b$ production in the 4F scheme matched to a parton shower [65]. Cross section uncertainties for $t\bar{t}+W$, $t\bar{t}+Z$ and $t\bar{t}+h_{\text{SM}}$ are taken to be 30% for each process. Uncertainties associated to jet energy and mass calibration are taken to be 5% per jet, fully correlated between energy and mass and across all jets in the event. Finally, uncertainties on the b -, c - and light-jet tagging efficiencies are taken to be 3%, 6% and 15% respectively. These uncertainties are taken as uncorrelated between b -jets, c -jets, and light-jets. As shown in Figs. 3 and 4, the resulting total background normalisation uncertainty is about 20%, although the different uncertainty components have different shape in the final distribution.

C. Statistical analysis

The BDRS jet mass distribution in the two analysis channels under consideration (see Figs. 3 and 4) are tested for the presence of a signal. To obtain the most realistic possible sensitivity projection, a sophisticated statistical analysis is performed, following very closely the strategy adopted in the experimental analyses at the LHC.

For each m_A hypothesis, 95% CL upper limits on the $t\bar{t}A$ production cross section times branching ratio, $\sigma(t\bar{t}A) \times \mathcal{B}(A \rightarrow b\bar{b})$, are obtained with the CL_s method [66, 67] using a profile likelihood ratio as test statistic implemented in the ROOFIT package [68, 69]. The likelihood function $\mathcal{L}(\mu, \theta)$ depends on the signal-strength parameter μ , a multiplicative factor to the theoretical signal production cross section, and θ , a set of nuisance parameters that encode the effect of systematic uncertainties in the analysis. The likelihood function is constructed as a product of Poisson probability terms over all bins of the distributions analysed, and of Gaussian or log-normal probability terms,

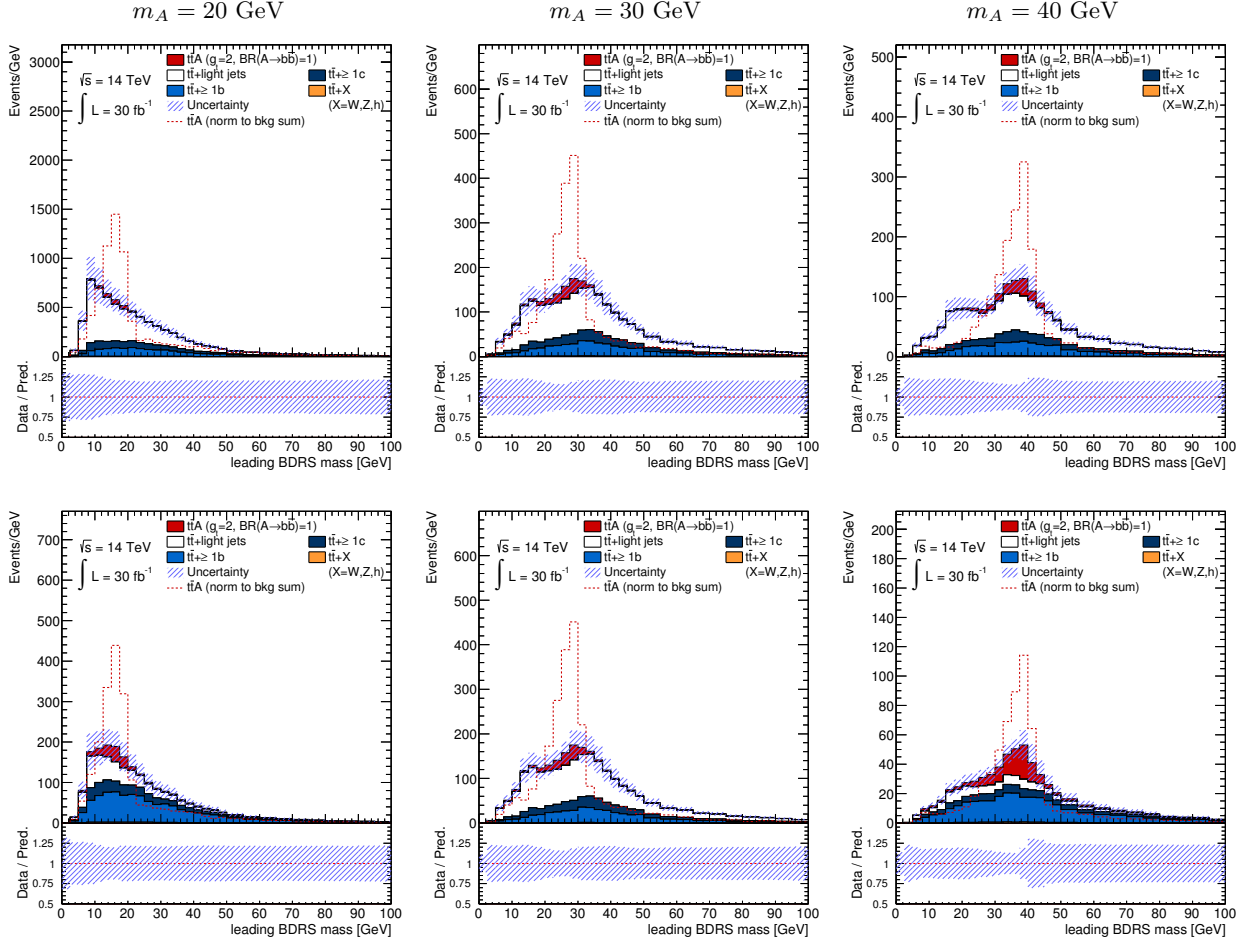


FIG. 3: Distribution of the leading BDRS jet mass in the two analysis channels considered after final selection: (top) ($\geq 5j$, $3b$) and (bottom) ($\geq 4j$, $\geq 4b$), for different values of m_A (20, 30 and 40 GeV). The prediction corresponds to $\sqrt{s} = 14$ TeV and an integrated luminosity of 30 fb^{-1} . Several background categories have been merged for visibility. The expected contribution from the ttA signal under the assumptions of $g_t = 2$ and $\mathcal{B}(A \rightarrow b\bar{b}) = 1$ is also shown (red histogram), stacked on top of the SM background. The dashed red line shows the ttA signal distribution normalised to the background yield to better compare the shape to that of the background. The bottom panel displays the expected total systematic uncertainty on the total prediction prior to the fit to the pseudo-data.

each corresponding to a nuisance parameter. For a given assumed value of μ , the profile likelihood ratio q_μ is defined as:

$$q_\mu = -2 \ln(\mathcal{L}(\mu, \hat{\theta}_\mu) / \mathcal{L}(\hat{\mu}, \hat{\theta})), \quad (3)$$

where $\hat{\theta}_\mu$ are the values of the nuisance parameters that maximise the likelihood function for a given value of μ , and $\hat{\mu}$ and $\hat{\theta}$ are the values of the parameters that maximise the likelihood function (with the constraint $0 \leq \hat{\mu} \leq \mu$). The maximisation of the likelihood function over the nuisance parameters allows variations of the expectations for signal and background in order to improve the agreement with (pseudo-)data, yielding a background prediction with reduced overall uncertainty and thus resulting in an improved sensitivity. For a given m_A hypothesis, values of the production cross section (parameterised by μ) yielding $\text{CL}_s < 0.05$, where CL_s is computed using the asymptotic approximation [70], are excluded at $\geq 95\%$ CL.

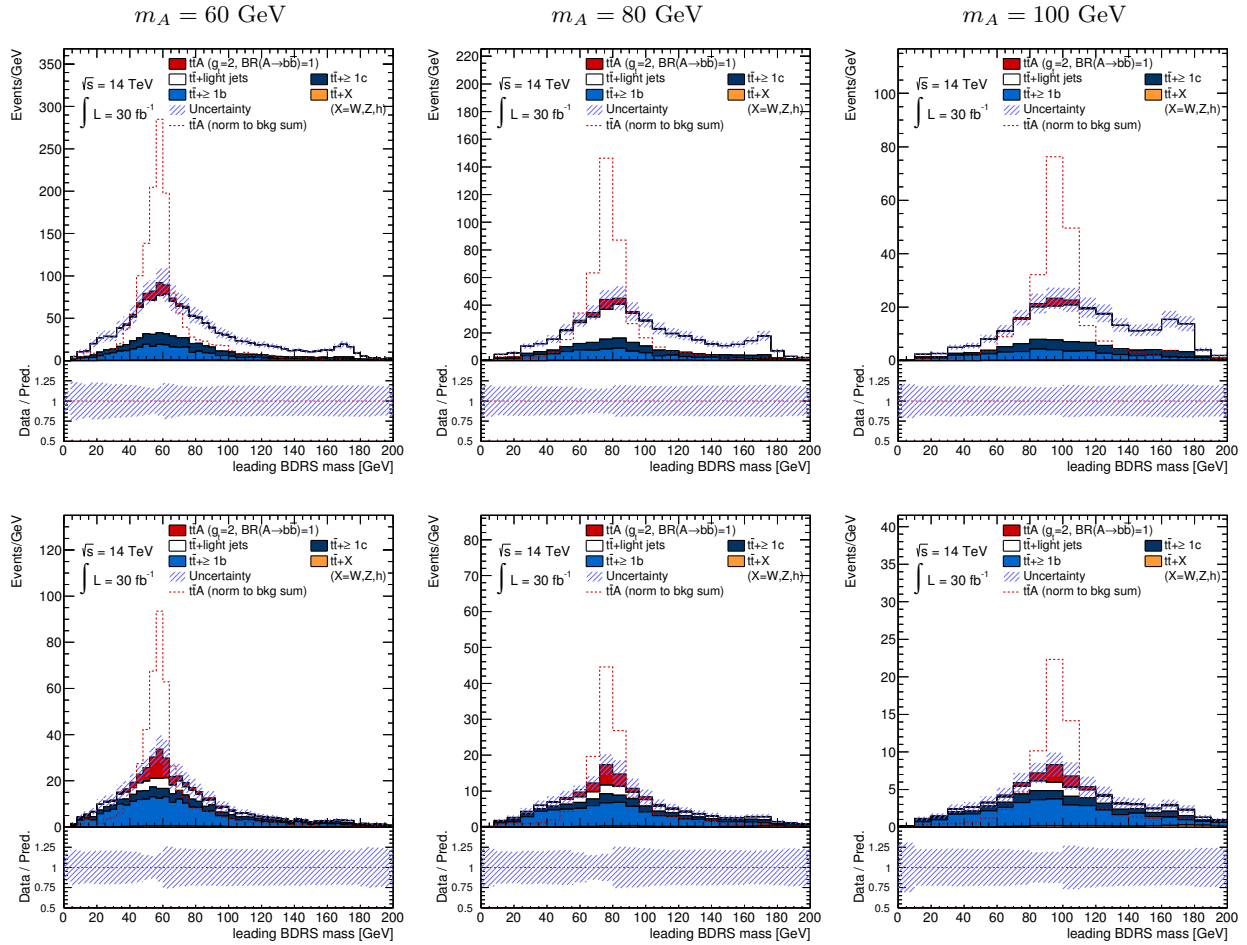


FIG. 4: Distribution of the leading BDRS jet mass in the two analysis channels considered after final selection: (top) $(\geq 5j, 3b)$ and (bottom) $(\geq 5j, \geq 4b)$, for different values of m_A (60, 80 and 100 GeV). The prediction corresponds to $\sqrt{s} = 14$ TeV and an integrated luminosity of 30 fb^{-1} . Several background categories have been merged for visibility. The expected contribution from the $t\bar{t}A$ signal under the assumptions of $g_t = 2$ and $\mathcal{B}(A \rightarrow b\bar{b}) = 1$ is also shown (red histogram), stacked on top of the SM background. The dashed red line shows the $t\bar{t}A$ signal distribution normalised to the background yield to better compare the shape to that of the background. The bottom panel displays the expected total systematic uncertainty on the total prediction prior to the fit to the pseudo-data.

V. ESTIMATED LIMITS ON A LIGHT CP-ODD SCALAR

Following the analyses steps and the limit setting outlined in Sects. II-IV, we estimate expected 95% CL upper limits on the production cross section times branching ratio, $\sigma(t\bar{t}A) \times \mathcal{B}(A \rightarrow b\bar{b})$, as a function of m_A (see Fig. 5). Table III summarises the 95% CL upper limits on $\sigma(t\bar{t}A) \times \mathcal{B}(A \rightarrow b\bar{b})$ as a function of m_A for different values of the integrated luminosity. Under the assumption $\mathcal{B}(A \rightarrow b\bar{b}) = 1$, the upper limits on $\sigma(t\bar{t}A) \times \mathcal{B}(A \rightarrow b\bar{b})$ can be translated on upper limits on $|g_t|$, which are summarised in Table IV.

Using the reconstruction strategy outlined in Sec. IV A, a CP-odd scalar that couples with $g_t = 1$ can be excluded for $20 \leq m_A \leq 90$ GeV with only 30 fb^{-1} of data (see Fig. 5). With an increased statistics of 300 fb^{-1} couplings as low as $g_t \simeq 0.5$ can be constrained over a large mass range, i.e. $30 \leq m_A \leq 80$ GeV.

VI. INTERPRETATION OF LIMITS

A light CP-odd Higgs boson ($m_A < 125$ GeV), which may or may not be related to global symmetries being present, exists in many extensions of the SM. Its couplings with gauge bosons are generically suppressed, yielding weak bounds

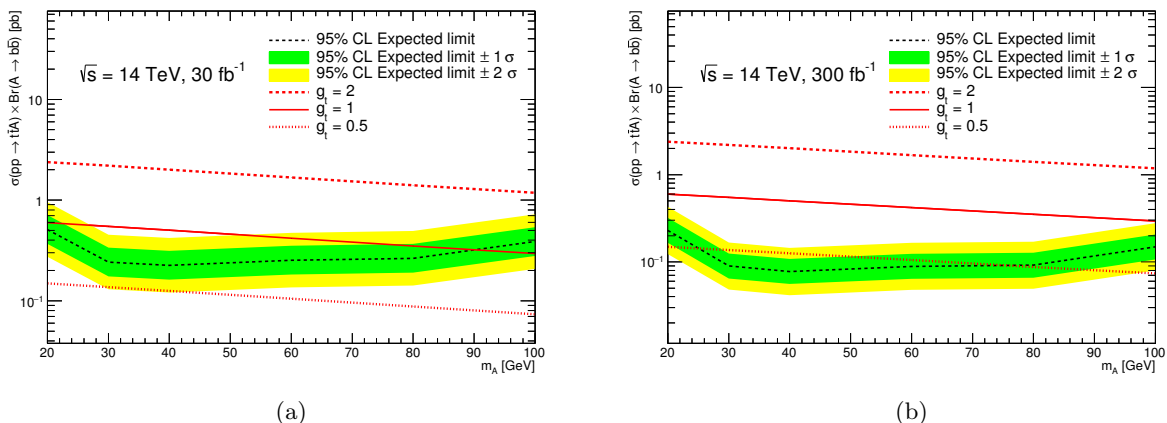


FIG. 5: Expected 95% CL upper limits on $\sigma(t\bar{t}A) \times \mathcal{B}(A \rightarrow b\bar{b})$ as a function of m_A in pp collisions at $\sqrt{s} = 14$ TeV for an integrated luminosity of (a) 30 fb^{-1} and (b) 300 fb^{-1} . The green and yellow bands correspond to 1 and 2 standard deviations respectively around the median expected limit under the background-only hypothesis. Also shown are the theoretical cross sections for $\sigma(t\bar{t}A)$ for different assumed values of g_t (0.5, 1.0 and 2.0) and $\mathcal{B}(A \rightarrow b\bar{b}) = 1$.

95% CL upper limits on $\sigma(t\bar{t}A) \times \mathcal{B}(A \rightarrow b\bar{b})$ (pb)						
\mathcal{L} (fb^{-1})	m_A (GeV)					
	20	30	40	60	80	100
1	4.46	2.50	2.38	2.57	2.78	3.94
30	1.02	0.48	0.45	0.51	0.53	0.78
100	0.67	0.29	0.25	0.29	0.30	0.46
300	0.46	0.18	0.16	0.18	0.18	0.30
3000	0.17	0.066	0.057	0.065	0.065	0.13

TABLE III: Expected 95% CL upper limits on $\sigma(t\bar{t}A) \times \mathcal{B}(A \rightarrow b\bar{b})$ as a function of m_A in pp collisions at $\sqrt{s} = 14$ TeV for different integrated luminosities.

95% CL upper limits on $ g_t $						
\mathcal{L} (fb^{-1})	m_A (GeV)					
	20	30	40	60	80	100
1	2.73	2.14	2.18	2.48	2.82	3.65
30	1.31	0.94	0.95	1.10	1.23	1.62
100	1.06	0.72	0.71	0.83	0.93	1.25
300	0.88	0.57	0.55	0.65	0.72	1.00
3000	0.54	0.35	0.34	0.39	0.43	0.67

TABLE IV: Expected 95% CL upper limits on $|g_t|$ as a function of m_A in pp collisions at $\sqrt{s} = 14$ TeV for different integrated luminosities, under the assumption $\mathcal{B}(A \rightarrow b\bar{b}) = 1$.

from LEP. If $m_A < m_{h_{\text{SM}}}/2$, it may be searched via the decay $h_{\text{SM}} \rightarrow AA$. Though such decay sometimes has a large branching ratio, being in conflict with current Higgs precision data, there do exist scenarios, in both supersymmetric and non-supersymmetric theories, where the $\mathcal{B}(h_{\text{SM}} \rightarrow AA)$ is suppressed. Therefore, new strategies for collider searches that could cover as large as possible model parameter space with a light CP-odd Higgs boson, are necessary. Next, we will interpret our collider analysis of $t\bar{t}A$ in several representative beyond-SM scenarios.

A. 2HDM

In the MSSM, a supersymmetric extension of a type-II 2HDM, a scenario with a light CP-odd Higgs boson is hard to achieve, given constraints from precision Higgs data. This is not surprising since there are only two free parameters at tree level in the Higgs sector, due to supersymmetric interrelations. The picture, however, is changed in the 2HDM without supersymmetry. With a softly-broken Z_2 symmetry ($\Phi_1 \rightarrow \Phi_1, \Phi_2 \rightarrow -\Phi_2$), which is often introduced to suppress scalar-mediated flavor changing processes, the Higgs potential of the 2HDM is given by:

$$V(\Phi_1, \Phi_2) = m_1^2 \Phi_1^\dagger \Phi_1 + m_2^2 \Phi_2^\dagger \Phi_2 + (m_{12}^2 \Phi_1^\dagger \Phi_2 + \text{h.c.}) + \frac{1}{2} \lambda_1 (\Phi_1^\dagger \Phi_1)^2 + \frac{1}{2} \lambda_2 (\Phi_2^\dagger \Phi_2)^2 \\ + \lambda_3 (\Phi_1^\dagger \Phi_1) (\Phi_2^\dagger \Phi_2) + \lambda_4 (\Phi_1^\dagger \Phi_2) (\Phi_2^\dagger \Phi_1) + \frac{1}{2} \lambda_5 [(\Phi_1^\dagger \Phi_2)^2 + \text{h.c.}]. \quad (4)$$

Here $\Phi_{1,2}$ are complex $SU(2)_L$ doublets. Assuming no CP-violation, the model has two CP-even and one CP-odd spin-0 neutral eigenstates, denoted as h, H , and A , respectively. Such a setup contains seven free parameters at tree level (including all Higgs masses), yielding a large parameter space that can accommodate a light CP-odd Higgs boson.

Theoretically, the 125 GeV SM-like Higgs boson h_{SM} could be either the light CP-even Higgs boson (h) or the heavy one (H). If $m_A < m_{h_{\text{SM}}}/2$, the decay $h_{\text{SM}} \rightarrow AA$ is kinematically allowed. Often the partial width for $h_{\text{SM}} \rightarrow AA$ becomes comparable or even dominant over that of $h_{\text{SM}} \rightarrow b\bar{b}$, given that the latter is suppressed by the lightness of the bottom quark. Therefore, $h_{\text{SM}} \rightarrow AA$ decays become a good probe for these light bosonic particles. However, as discussed recently [71],² in the alignment limit [$\cos(\beta - \alpha) = 0$ if $h_{\text{SM}} = h$, and $\sin(\beta - \alpha) = 0$ if $h_{\text{SM}} = H$], which is favoured by current precision Higgs measurements, the Higgs coupling $g_{h_{\text{SM}}AA}$ is reduced to:

$$|g_{h_{\text{SM}}AA}| = \left| -\frac{2m_A^2 + m_{h_{\text{SM}}}^2 - 4m_{12}^2/\sin 2\beta}{v} \right|. \quad (5)$$

In case that $2m_A^2 + m_{h_{\text{SM}}}^2 \sim 4m_{12}^2/\sin 2\beta$, the decay $h_{\text{SM}} \rightarrow AA$ would be greatly suppressed. Therefore, collider strategies are needed to probe these scenarios with $m_A < m_{\text{SM}}/2$, as well as the scenarios with $m_A > m_{\text{SM}}/2$.

We should note that the perturbation requirement for Higgs couplings yields bounds on $\tan \beta$. Particularly, the coupling λ_1 is related to the Higgs boson mass via the relation [71]:

$$\lambda_1 = \frac{m_h^2 + m_H^2 \tan^2 \beta - m_{12}^2 (\tan \beta + \tan^3 \beta)}{v^2}. \quad (6)$$

Assuming $g_{h_{\text{SM}} \rightarrow AA} = 0$, it becomes:

$$\lambda_1 = \frac{m_h^2 + \tan^2 \beta (m_H^2 - m_{h_{\text{SM}}}^2/2 - m_A^2)}{v^2}. \quad (7)$$

Given $m_H^2 - m_{h_{\text{SM}}}^2/2 - m_A^2 > 0$ for $m_A < m_{h_{\text{SM}}}/2$, the perturbativity condition $\lambda_1 < 4\pi$ immediately sets an upper bound for $\tan \beta$ in this region:

$$\tan \beta < \sqrt{\frac{4\pi v^2 - m_h^2}{m_H^2 - m_{h_{\text{SM}}}^2/2 - m_A^2}} < \sqrt{\frac{4\pi v^2}{m_{h_{\text{SM}}}^2/2 - m_A^2}} \sim 10 - 20. \quad (8)$$

These features are illustrated in Fig. 6. Additionally, the perturbation requirement for top Yukawa couplings can bound the $\tan \beta$ value from below. So we will limit our discussions for $\tan \beta > 0.1$.

The expected sensitivities for probing these scenarios in the 2HDM via $b\bar{b}A$ and $t\bar{t}A$ production are presented in Fig. 7. For illustration, we focus on type-I and type-II 2HDMs. The $b\bar{b}A$ reach is estimated based on the projections from Ref. [73], neglecting systematic uncertainties. Within a type-II 2HDM, the $t\bar{t}A$ and $b\bar{b}A$ channels are complementary to each other in searching for light CP-odd Higgs bosons, since the coupling g_{bbA} is $\tan \beta$ -enhanced whereas g_{ttA} is $\cot \beta$ -enhanced. With integrated luminosities in excess of 300 fb^{-1} , the whole parameter region can be covered except a corner with relatively large m_A and moderate $\tan \beta$. This is interesting given that low $\tan \beta$ is particularly favoured by perturbativity. In contrast, within a type-I 2HDM, the coupling g_{bbA} would also be $\cot \beta$ -enhanced, so

² See Refs. [12, 72] for discussions in the context of the NMSSM.

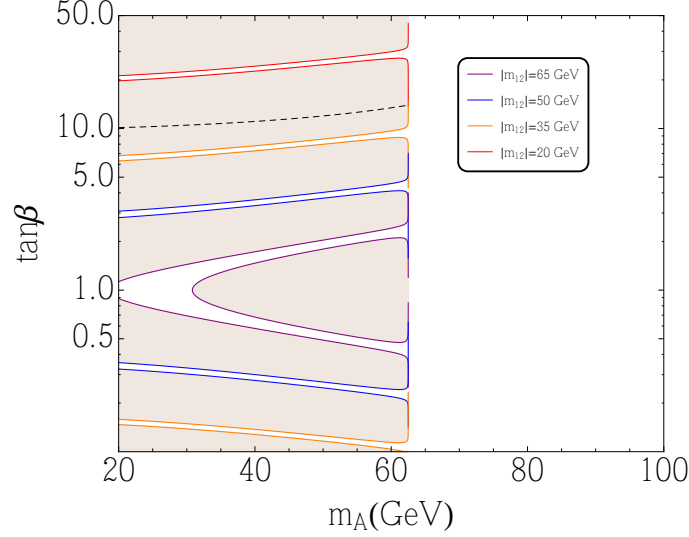


FIG. 6: Parameter region with $\mathcal{B}(h_{\text{SM}} \rightarrow AA) < 30\%$ in the 2HDM (blank region). The blank belts in the region with $m_A < m_{h_{\text{SM}}}/2$, which are characterised by different boundary colours, are yielded by different m_{12}^2 values. The black dashed line represents a universal upper limit on $\tan\beta$ due to the perturbation requirement for λ_1 .

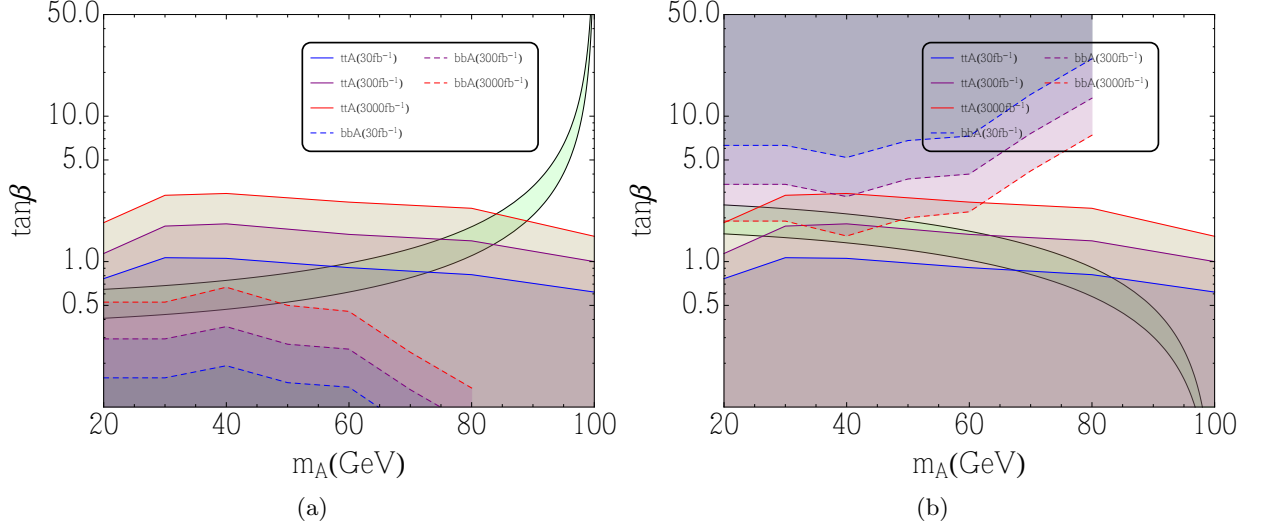


FIG. 7: Sensitivity reach (at 95% CL) of the $b\bar{b}A$ and $t\bar{t}A$ channels within the (a) type-I 2HDM and (b) type-II 2HDM. The green bands represent a region where the recently observed gamma-ray excess from the Galactic Centre can be explained, yielding a DM annihilation cross section of $\langle\sigma v\rangle \simeq 1 - 2.5 \times 10^{-26} \text{cm}^3 \text{s}^{-1}$. Here the DM particle mass $m_\chi = 50 \text{ GeV}$ and the coupling between the mediator and the DM particles $y_\chi = 0.3$ are assumed.

both search channels are no longer probing complementary $\tan\beta$ regions. As a matter of fact, in such scenario the $t\bar{t}A$ channel provides a better sensitivity to search for the light CP-odd Higgs boson over the whole mass range of $20 \text{ GeV} < m_A < 100 \text{ GeV}$, although the high- $\tan\beta$ region remains difficult to probe.

Searches for $t\bar{t}A$ and $b\bar{b}A$ also provide a probe for DM physics. For example, consider a Dirac fermion χ that is a DM candidate, with mass m_χ , and coupling to the CP-odd scalar A via:

$$\mathcal{L} \supset y_\chi A \bar{\chi} i \gamma^5 \chi. \quad (9)$$

Integrating out A yields a dimension-six effective operator:

$$\mathcal{L}_{\text{eff}} \sim \frac{-y_b y_\chi m_b}{\Lambda^3} \bar{\chi} \gamma^5 \chi \bar{b} \gamma^5 b. \quad (10)$$

Such an operator implies s-wave DM annihilation $\chi\chi \rightarrow b\bar{b}$ with

$$\langle\sigma v\rangle = \frac{3}{8\pi} \frac{y_\chi^2 g_b^2 y_b^2 m_\chi^2}{(m_A^2 - 4m_\chi^2)^2 + m_A^2 \Gamma_A^2} \sqrt{1 - \frac{m_b^2}{m_\chi^2}}, \quad (11)$$

allowing an explanation for the recently observed diffuse gamma-ray excess from the Galactic Centre [4, 74], and a spin-dependent and p-wave-suppressed direct detection signal, resulting in a weak bound from current direct detection searches. In Fig. 7, the $\tan\beta - m_A$ values consistent with an explanation of the gamma-ray excess are indicated, yielding a DM annihilation cross section of $\langle\sigma v\rangle \simeq 1 - 2.5 \times 10^{-26} \text{cm}^3 \text{s}^{-1}$, with $m_\chi = 50 \text{ GeV}$ [75] and $y_\chi = 0.3$ assumed. In this scenario, monojet searches at the LHC would also be insensitive since the decay $A \rightarrow \chi\chi$ would be kinematically forbidden, while the $t\bar{t}A$, $A \rightarrow b\bar{b}$ search would provide an effective probe.

B. NMSSM

Another class of benchmark scenarios for light CP-odd Higgs bosons arise in the NMSSM, with the superpotential and soft supersymmetry-breaking terms of its Higgs sector given by

$$\begin{aligned} \mathbf{W} &= \lambda \mathbf{S} \mathbf{H}_d \mathbf{H}_u + \frac{1}{3} \kappa \mathbf{S}^3, \\ V_{\text{soft}} &= m_{H_d}^2 |H_d|^2 + m_{H_u}^2 |H_u|^2 + m_S^2 |S|^2 - (\lambda A_\lambda H_u H_d S + \text{h.c.}) + \left(\frac{1}{3} \kappa A_\kappa S^3 + \text{h.c.}\right), \end{aligned} \quad (12)$$

where H_d , H_u and S denote the neutral Higgs fields of the \mathbf{H}_d , \mathbf{H}_u and \mathbf{S} supermultiplets, respectively. For convenience, let's define its CP-even and CP-odd mass eigenstates as H_i , $i = 1, 2, 3$, and A_j , $j = 1, 2$, respectively.

In contrast with the 2HDM case, the light CP-odd Higgs boson in the NMSSM often results from breaking an approximate global symmetry spontaneously, serving as an axion or a pseudo-Goldstone boson. Its appearance is thus less ‘‘artificial’’. Let us start with the tree-level mass matrix of the CP-odd Higgs bosons in the NMSSM:

$$\mathcal{M}_P^2 = \begin{pmatrix} m_A^2 & \lambda v \left(\frac{m_A^2}{2\mu} \sin 2\beta - \frac{3\kappa\mu}{\lambda} \right) \\ \lambda^2 v^2 s_{2\beta} \left(\frac{m_A^2}{4\mu^2} \sin 2\beta + \frac{3\kappa}{2\lambda} \right) - \frac{3\kappa A_\kappa \mu}{\lambda} & m_A^2 = \frac{2\mu(A_\lambda + \kappa S)}{\sin 2\beta} \end{pmatrix}, \quad (13)$$

which yields a determinant

$$\det(\mathcal{M}_P^2) = 9\kappa\lambda v^2 \mu A_\lambda - \frac{6A_\kappa \kappa \mu^2}{\lambda \sin 2\beta} \left(A_\lambda + \frac{\kappa\mu}{\lambda} \right). \quad (14)$$

Necessarily, the scenarios with a light A_1 (A_1 denotes the lightest CP-odd Higgs boson) or $m_{A_1} \rightarrow 0$ yield $\det(\mathcal{M}_P^2) \rightarrow 0$ and viceversa, if such a stable vacuum exists. Among various possibilities, two have been studied extensively: R-symmetry (or R-limit) and Peccei-Quinn (PQ) symmetry (or PQ-limit), both of which yield a vanishing determinant at tree level. Another difference between these two class of scenarios is that the light CP-odd Higgs boson in the NMSSM is typically singlet-like. This can be understood since the Goldstone boson of a spontaneously-broken global $U(1)$ symmetry is manifested as

$$A_1 \sim \sum_i \frac{q_i v_i}{v_{U(1)}} \Phi_i, \quad \Phi_i = S, H_u, H_d. \quad (15)$$

Here $v_{U(1)} = \sqrt{\sum_i q_i^2 v_i^2}$ is the $U(1)$ breaking scale and q_i is the $U(1)$ charge of Φ_i . An effective parameter $\mu = \lambda \langle v_S \rangle$ of the electroweak scale with $\lambda \sim \mathcal{O}(0.1)$ naturally yields $v_S \gg v_u, v_d$, and hence a singlet-like pseudo-Goldstone boson. This feature renders such a light boson much more difficult to probe at colliders, compared to the 2HDM case. Next, we will evaluate the collider constraints on these two scenarios.

1. R-limit: $A_\lambda \rightarrow 0$, $A_\kappa \rightarrow 0$, where the theory is approximately invariant under the transformation

$$H_u \rightarrow H_u \exp(i\phi_R), \quad H_d \rightarrow H_d \exp(i\phi_R), \quad S \rightarrow S \exp(i\phi_R), \quad (16)$$

and the tree-level couplings of the R-axion A_1 with the top and bottom quarks are given by

$$y_{A_1 tt} = \frac{2\lambda v \cos^2 \beta}{\mu}, \quad y_{A_1 bb} = \frac{2\lambda v \sin^2 \beta}{\mu}. \quad (17)$$

In this scenario, both λ and κ can be large, yielding a sizeable contribution to the mass of the SM-like Higgs boson at tree level. Hence, a large value for $\tan\beta$ is unnecessary. A scan in the parameter space in this scenario is performed using NMSSMTools 4.2.1 [76] including all built-in constraints, such as from Higgs searches, superpartner searches, muon $g-2$, flavour physics, invisible Z -decay, and the constraints from Υ decays (with the exception of the Landau pole test and DM related-constraints, which are not considered). The resulting values for the $y_{A_1 tt}$ and $y_{A_1 bb}$ couplings are compared to the expected collider bounds in Fig. 8(a). Depending on the parameter values, the magnitude of $y_{A_1 tt}$ in this scenario can be up to ~ 0.5 . Only for an integrated luminosity of 3000 fb^{-1} the LHC can probe a coupling $y_{A_1 tt}$ as small as 0.5 via the $t\bar{t}A_1$, $A_1 \rightarrow b\bar{b}$ channel. Therefore this scenario is difficult to probe, even at the HL-LHC.

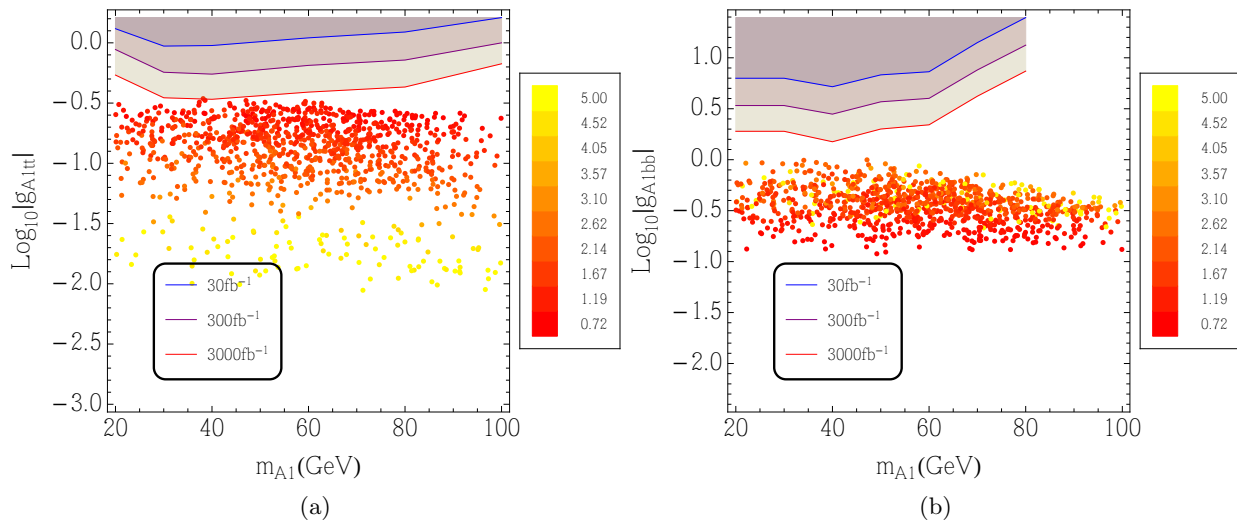


FIG. 8: Sensitivity reach (at 95% CL) to the R-limit scenario in the NMSSM via the (a) $t\bar{t}A_1$ and (b) $b\bar{b}A_1$ channels. The scan is over all parameters, in the ranges $0.1 \leq \lambda \leq 0.6$, $0.1 \leq \kappa \leq 0.6$, $-7 \leq A_\lambda \leq 7 \text{ GeV}$, $-7 \leq A_\kappa \leq 0 \text{ GeV}$, $0.1 \leq \tan\beta \leq 5$, and $100 \leq \mu \leq 500 \text{ GeV}$. We have assumed soft squark masses of 2 TeV, slepton masses of 200 GeV, $A_{u,d,e} = -3.5 \text{ TeV}$, and bino, wino and gluino masses of 100, 200, and 2000 GeV, respectively. The hue of the scatter points represents the correspondent $\tan\beta$ values.

2. PQ-limit: $\frac{\kappa}{\lambda} \rightarrow 0$, $A_\kappa \rightarrow 0$, where the theory is approximately invariant under the transformation

$$H_u \rightarrow H_u \exp(i\phi_{\text{PQ}}), \quad H_d \rightarrow H_d \exp(i\phi_{\text{PQ}}), \quad S \rightarrow S \exp(-2i\phi_{\text{PQ}}), \quad (18)$$

and the tree-level mass of the PQ pseudo-Goldstone boson A_1 are given given by

$$m_{A_1} = -\frac{3\kappa A_\kappa \mu}{\lambda}. \quad (19)$$

This scenario has been proposed as a supersymmetric benchmark for sub-electroweak scale (singlino-like) DM [72], since its lightest neutralino is generically singlino-like and lighter than the electroweak scale. Particularly, in this scenario A_1 can serve as the mediator for DM annihilation into a bottom quark pair and explain the diffuse gamma-ray excess from the Galactic Centre [11, 12]. In this limit, the tree-level couplings of A_1 with the top and bottom quarks are given by

$$y_{A_1 tt} = \frac{\lambda v \cos^2 \beta}{\mu}, \quad y_{A_1 bb} = \frac{\lambda v \sin^2 \beta}{\mu}, \quad (20)$$

and so smaller by a factor of two than the corresponding couplings in the R-limit. Furthermore, a smaller λ is favoured in this limit and a relatively large $\tan\beta$ is needed to generate a mass of 125 GeV for the SM-like Higgs boson. Therefore, the coupling $y_{A_1 tt}$ tends to be smaller than in the R-limit scenario. The resulting values for the $y_{A_1 tt}$ and $y_{A_1 bb}$ couplings are compared to the expected collider bounds in Fig. 8(b). For most of the points, the magnitude of $y_{A_1 tt}$ is below 0.1, which renders this scenario extremely difficult to probe at the using the

$t\bar{t}A_1$ channel.³

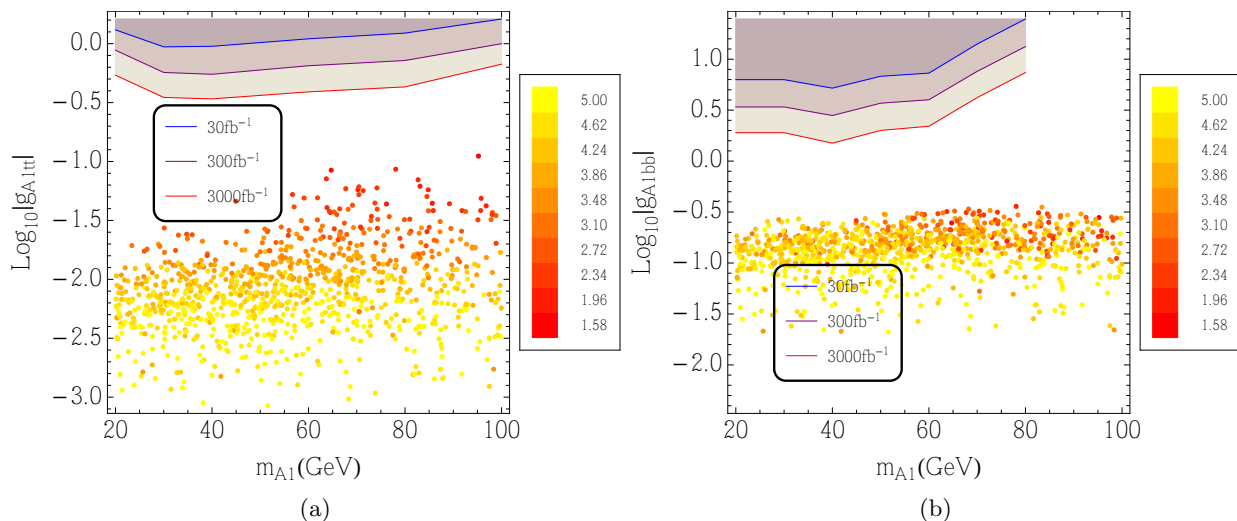


FIG. 9: Sensitivity reach (at 95% CL) to the PQ-limit scenario in the NMSSM via the (a) $t\bar{t}A_1$ and (b) $b\bar{b}A_1$ channels. The scan is over all parameters, in the ranges $0.06 \leq \lambda \leq 0.6$, $5 \leq \kappa/\lambda \leq 100$, $|\varepsilon'| = |A_\lambda/\mu \tan\beta - 1| \leq 0.25$, $-100 \leq A_\kappa \leq 0$ GeV, $0.1 \leq \tan\beta \leq 5$, and $100 \leq \mu \leq 500$ GeV. We have assumed soft squark masses of 2 TeV, slepton masses of 200 GeV, $A_{u,d,e} = 3.5$ TeV, and bino, wino and gluino masses of 100, 200, and 2000 GeV, respectively. The hue of the scatter points represents the correspondent $\tan\beta$ values.

Finally, we stress that the $b\bar{b}A_1$ channel doesn't help much in probing the R- and PQ-limit scenarios. The sensitivities of both searches are suppressed by the mixture with the singlet. Even worse, the mixing is approximately $\tan\beta$ enhanced, further suppressing the sensitivity of the $b\bar{b}A_1$ in probing the large $\tan\beta$ region in both scenarios.

VII. CONCLUSIONS

Searches for CP-odd scalars, as predicted by many extensions of the Standard Model and motivated by some recent astroparticle observations, are part of the core program of upcoming LHC runs at $\sqrt{s} = 13$ and 14 TeV. Searches at LEP and during Run 1 of the LHC at $\sqrt{s} = 7$ and 8 TeV have placed only weak constraints on the coupling strengths of CP-odd scalars with top and bottom quarks, or in their allowed mass range.

Using a simplified model approach for the signal, we have carried out a detailed study to evaluate the prospects at the LHC for probing scenarios with a CP-odd scalar with mass $20 \leq m_A < 100$ GeV, via the process $pp \rightarrow t\bar{t}A$ with subsequent decay $A \rightarrow b\bar{b}$. To separate the signal from the large background from $t\bar{t}$ +jets production, we apply jet substructure techniques, reconstructing the mass of the CP-odd scalar as the mass of a large-radius jet containing two b -tagged subjets. The chosen method allows for a so-called 'bump hunt' over a fairly smooth background, and it may be the most promising strategy for searching for a CP-odd scalar with mass $\lesssim 50$ GeV, i.e. about twice the typical minimum p_T cut for narrow jets used in standard LHC searches. A significant effort has been made in developing a semi-realistic experimental analysis, including a fairly complete description of systematic uncertainties and the usage of sophisticated statistical tools to constrain *in-situ* the effect of systematic uncertainties, thus limiting their impact on the search sensitivity. We then derive expected upper limits on the production cross section times branching ratio using the CL_s method.

In specific models, e.g. 2HDM or NMSSM, the coupling of the A boson with the top quark is related to other couplings in a well-defined way. Hence, the upper limits obtained on this coupling for a given mass m_A , can be used to bound other couplings of these models indirectly or as input for a global coupling fit. We find that in a type-I and type-II 2HDM the LHC can constrain a large fraction of the $(m_A, \tan\beta)$ parameter space, including the region preferred to explain the diffuse gamma-ray excess from the Galactic Centre as dark-matter annihilation via a CP-odd

³ For alternative way to probing this scenario, using exotic Higgs decays, see e.g. Ref. [12, 77, 78].

scalar mediator and decaying into $b\bar{b}$. However, in the case of the NMSSM with a light CP-odd scalar, a Goldstone boson of either a spontaneously-broken R- or PQ-symmetry, the LHC appears to have very limited sensitivity in probing these models.

Hence, depending on the concrete embedding of the scalar sector into a UV-complete theory, the LHC can provide complementary information, not accessible at either indirect detection experiments or electron-positron colliders, on the existence of CP-odd scalars, their mass and couplings to third-generation fermions.

VIII. ACKNOWLEDGMENTS

This research was supported in part by the European Commission through the 'HiggsTools' Initial Training Network PITN-GA-2012-316704 (M.S.) and by the Spanish Ministerio de Economía y Competitividad under projects FPA2012-38713 and Centro de Excelencia Severo Ochoa SEV-2012-0234 (M.C., T.F. and A.J). T.L. is supported by his start-up fund at the HKUST. T.L. would also like to thank Y. Jiang for useful discussions and acknowledge the hospitality of the Jockey Club Institute for Advanced Study, HKUST, where part of this work was completed.

-
- [1] S. Chatrchyan *et al.* [CMS Collaboration], Phys. Lett. B **716** (2012) 30.
 - [2] G. Aad *et al.* [ATLAS Collaboration], Phys. Lett. B **716** (2012) 1.
 - [3] F. Englert and R. Brout, Phys. Rev. Lett. **13** (1964) 321. P. W. Higgs, Phys. Lett. **12** (1964) 132 and Phys. Rev. Lett. **13** (1964) 508. G. S. Guralnik, C. R. Hagen and T. W. B. Kibble, Phys. Rev. Lett. **13** (1964) 585.
 - [4] L. Goodenough and D. Hooper, arXiv:0910.2998 [hep-ph].
 - [5] D. Hooper and L. Goodenough, Phys. Lett. B **697**, 412 (2011) [arXiv:1010.2752 [hep-ph]].
 - [6] K. N. Abazajian and M. Kaplinghat, Phys. Rev. D **86**, 083511 (2012) [Phys. Rev. D **87**, 129902 (2013)] [arXiv:1207.6047 [astro-ph.HE]].
 - [7] T. Daylan, D. P. Finkbeiner, D. Hooper, T. Linden, S. K. N. Portillo, N. L. Rodd and T. R. Slatyer, arXiv:1402.6703 [astro-ph.HE].
 - [8] C. Boehm, M. J. Dolan, C. McCabe, M. Spannowsky and C. J. Wallace, JCAP **1405**, 009 (2014) [arXiv:1401.6458 [hep-ph]].
 - [9] A. Hektor and L. Marzola, Phys. Rev. D **90**, no. 5, 053007 (2014) [arXiv:1403.3401 [hep-ph]].
 - [10] C. Arina, E. Del Nobile and P. Panci, Phys. Rev. Lett. **114**, 011301 (2015) [arXiv:1406.5542 [hep-ph]].
 - [11] C. Cheung, M. Papucci, D. Sanford, N. R. Shah and K. M. Zurek, Phys. Rev. D **90**, no. 7, 075011 (2014) [arXiv:1406.6372 [hep-ph]].
 - [12] J. Huang, T. Liu, L. T. Wang and F. Yu, Phys. Rev. D **90**, no. 11, 115006 (2014) [arXiv:1407.0038 [hep-ph]].
 - [13] S. Malik, C. McCabe, H. Araujo, A. Belyaev, C. Boehm, J. Brooke, O. Buchmueller and G. Davies *et al.*, arXiv:1409.4075 [hep-ex].
 - [14] J. Abdallah, A. Ashkenazi, A. Boveia, G. Busoni, A. De Simone, C. Doglioni, A. Efrati and E. Etzion *et al.*, arXiv:1409.2893 [hep-ph].
 - [15] N. Craig, F. D'Eramo, P. Draper, S. Thomas and H. Zhang, JHEP **1506**, 137 (2015) [arXiv:1504.04630 [hep-ph]].
 - [16] J. Hajer, Y. Y. Li, T. Liu and J. F. H. Shiu, arXiv:1504.07617 [hep-ph].
 - [17] M. J. Dolan, C. McCabe, F. Kahlhoefer and K. Schmidt-Hoberg, JHEP **1503**, 171 (2015) [arXiv:1412.5174 [hep-ph]].
 - [18] G. D'Ambrosio, G. F. Giudice, G. Isidori and A. Strumia, Nucl. Phys. B **645**, 155 (2002) [hep-ph/0207036].
 - [19] G. Klamke and D. Zeppenfeld, JHEP **0704**, 052 (2007) [hep-ph/0703202 [HEP-PH]].
 - [20] M. J. Dolan, P. Harris, M. Jankowiak and M. Spannowsky, Phys. Rev. D **90**, no. 7, 073008 (2014) [arXiv:1406.3322 [hep-ph]].
 - [21] D. Alves *et al.* [LHC New Physics Working Group Collaboration], J. Phys. G **39**, 105005 (2012) [arXiv:1105.2838 [hep-ph]].
 - [22] M. R. Buckley, D. Feld and D. Goncalves, Phys. Rev. D **91**, no. 1, 015017 (2015) [arXiv:1410.6497 [hep-ph]].
 - [23] P. Harris, V. V. Khoze, M. Spannowsky and C. Williams, Phys. Rev. D **91**, no. 5, 055009 (2015) [arXiv:1411.0535 [hep-ph]].
 - [24] U. Haisch and E. Re, JHEP **1506**, 078 (2015) [arXiv:1503.00691 [hep-ph]].
 - [25] V. V. Khoze, G. Ro and M. Spannowsky, arXiv:1505.03019 [hep-ph].
 - [26] J. Alwall, M. Herquet, F. Maltoni, O. Mattelaer and T. Stelzer, JHEP **1106**, 128 (2011) [arXiv:1106.0522 [hep-ph]].
 - [27] P. M. Nadolsky, H. L. Lai, Q. H. Cao, J. Huston, J. Pumplin, D. Stump, W. K. Tung and C.-P. Yuan, Phys. Rev. D **78** (2008) 013004 [arXiv:0802.0007 [hep-ph]].
 - [28] T. Sjostrand, S. Mrenna and P. Z. Skands, JHEP **0605** (2006) 026 [hep-ph/0603175].
 - [29] P. Z. Skands, Phys. Rev. D **82** (2010) 074018 [arXiv:1005.3457 [hep-ph]].
 - [30] A. Alloul, N. D. Christensen, C. Degrande, C. Duhr and B. Fuks, Comput. Phys. Commun. **185** (2014) 2250 [arXiv:1310.1921 [hep-ph]].
 - [31] C. Degrande, C. Duhr, B. Fuks, D. Grellscheid, O. Mattelaer and T. Reiter, Comput. Phys. Commun. **183** (2012) 1201 [arXiv:1108.2040 [hep-ph]].
 - [32] R. Frederix, S. Frixione, V. Hirschi, F. Maltoni, R. Pittau and P. Torrielli, Phys. Lett. B **701**, 427 (2011) [arXiv:1104.5613 [hep-ph]].

- [33] M. L. Mangano, M. Moretti and R. Pittau, Nucl. Phys. B **632** (2002) 343 [hep-ph/0108069].
- [34] M. Czakon and A. Mitov, Comput. Phys. Commun. **185** (2014) 2930 [arXiv:1112.5675 [hep-ph]].
- [35] M. Cacciari, M. Czakon, M. Mangano, A. Mitov and P. Nason, Phys. Lett. B **710** (2012) 612 [arXiv:1111.5869 [hep-ph]].
- [36] P. Brnreuther, M. Czakon and A. Mitov, Phys. Rev. Lett. **109** (2012) 132001 [arXiv:1204.5201 [hep-ph]].
- [37] M. Czakon and A. Mitov, JHEP **1212** (2012) 054 [arXiv:1207.0236 [hep-ph]].
- [38] M. Czakon and A. Mitov, JHEP **1301** (2013) 080 [arXiv:1210.6832 [hep-ph]].
- [39] M. Czakon, P. Fiedler and A. Mitov, Phys. Rev. Lett. **110** (2013) 252004 [arXiv:1303.6254 [hep-ph]].
- [40] A. D. Martin, W. J. Stirling, R. S. Thorne and G. Watt, Eur. Phys. J. C **63** (2009) 189 [arXiv:0901.0002 [hep-ph]].
- [41] A. D. Martin, W. J. Stirling, R. S. Thorne and G. Watt, Eur. Phys. J. C **64** (2009) 653 [arXiv:0905.3531 [hep-ph]].
- [42] M. Cacciari, G. P. Salam and G. Soyez, JHEP **0804** (2008) 063 [arXiv:0802.1189 [hep-ph]].
- [43] M. Cacciari and G. P. Salam, Phys. Lett. B **641** (2006) 57 [hep-ph/0512210].
- [44] M. Cacciari, G. P. Salam and G. Soyez, Eur. Phys. J. C **72** (2012) 1896 [arXiv:1111.6097 [hep-ph]].
- [45] G. Aad *et al.* [ATLAS Collaboration], arXiv:1503.05066 [hep-ex].
- [46] M. V. Garzelli, A. Kardos, C. G. Papadopoulos and Z. Trocsanyi, JHEP **1211** (2012) 056 [arXiv:1208.2665 [hep-ph]].
- [47] S. Dawson, C. Jackson, L. H. Orr, L. Reina and D. Wackerroth, Phys. Rev. D **68** (2003) 034022 [hep-ph/0305087].
- [48] W. Beenakker, S. Dittmaier, M. Kramer, B. Plumper, M. Spira and P. M. Zerwas, Nucl. Phys. B **653** (2003) 151 [hep-ph/0211352].
- [49] W. Beenakker, S. Dittmaier, M. Kramer, B. Plumper, M. Spira and P. M. Zerwas, Phys. Rev. Lett. **87** (2001) 201805 [hep-ph/0107081].
- [50] A. Djouadi, J. Kalinowski and M. Spira, Comput. Phys. Commun. **108** (1998) 56 [hep-ph/9704448].
- [51] A. Bredenstein, A. Denner, S. Dittmaier and M. M. Weber, Phys. Rev. D **74** (2006) 013004 [hep-ph/0604011].
- [52] S. Actis, G. Passarino, C. Sturm and S. Uccirati, Nucl. Phys. B **811** (2009) 182 [arXiv:0809.3667 [hep-ph]].
- [53] A. Denner, S. Heinemeyer, I. Puljak, D. Rebuszi and M. Spira, Eur. Phys. J. C **71** (2011) 1753 [arXiv:1107.5909 [hep-ph]].
- [54] S. Dittmaier *et al.* [LHC Higgs Cross Section Working Group Collaboration], arXiv:1101.0593 [hep-ph].
- [55] M. Cacciari and G. P. Salam, Phys. Lett. B **659** (2008) 119 [arXiv:0707.1378 [hep-ph]].
- [56] M. Cacciari, G. P. Salam and G. Soyez, JHEP **0804** (2008) 005 [arXiv:0802.1188 [hep-ph]].
- [57] Y. L. Dokshitzer, G. D. Leder, S. Moretti and B. R. Webber, JHEP **9708** (1997) 001 [hep-ph/9707323].
- [58] M. Wobisch and T. Wengler, In *Hamburg 1998/1999, Monte Carlo generators for HERA physics* 270-279 [hep-ph/9907280].
- [59] J. M. Butterworth, A. R. Davison, M. Rubin and G. P. Salam, Phys. Rev. Lett. **100** (2008) 242001 [arXiv:0802.2470 [hep-ph]].
- [60] T. Plehn, G. P. Salam and M. Spannowsky, Phys. Rev. Lett. **104**, 111801 (2010) [arXiv:0910.5472 [hep-ph]].
- [61] G. Aad *et al.* [ATLAS Collaboration], JHEP **1309** (2013) 076 [arXiv:1306.4945 [hep-ex]].
- [62] V. Khachatryan *et al.* [CMS Collaboration], Eur. Phys. J. C **75** (2015) 6, 251 [arXiv:1502.02485 [hep-ex]].
- [63] G. Aad *et al.* [ATLAS Collaboration], arXiv:1505.04306 [hep-ex].
- [64] S. Hoeche, F. Krauss, P. Maierhofer, S. Pozzorini, M. Schonherr and F. Siegert, arXiv:1402.6293 [hep-ph].
- [65] F. Cascioli, P. Maierhofer, N. Moretti, S. Pozzorini and F. Siegert, Phys. Lett. B **734** (2014) 210 [arXiv:1309.5912 [hep-ph]].
- [66] T. Junk, Nucl. Instrum. Meth. A **434** (1999) 435 [hep-ex/9902006].
- [67] A. L. Read, J. Phys. G **28** (2002) 2693.
- [68] W. Verkerke and D. P. Kirkby, eConf C **0303241** (2003) MOLT007 [physics/0306116].
- [69] W. Verkerke and D. P. Kirkby, <http://roofit.sourceforge.net/>.
- [70] G. Cowan, K. Cranmer, E. Gross and O. Vitells, Eur. Phys. J. C **71** (2011) 1554 [Eur. Phys. J. C **73** (2013) 2501] [arXiv:1007.1727 [physics.data-an]].
- [71] J. Bernon, J. F. Gunion, Y. Jiang and S. Kraml, Phys. Rev. D **91**, no. 7, 075019 (2015) [arXiv:1412.3385 [hep-ph]].
- [72] P. Draper, T. Liu, C. E. M. Wagner, L. T. Wang and H. Zhang, Phys. Rev. Lett. **106**, 121805 (2011) [arXiv:1009.3963 [hep-ph]].
- [73] J. Kozaczuk and T. A. W. Martin, JHEP **1504**, 046 (2015) [arXiv:1501.07275 [hep-ph]].
- [74] V. Vitale *et al.* [Fermi-LAT Collaboration], arXiv:0912.3828 [astro-ph.HE].
- [75] F. Calore, I. Cholis, C. McCabe and C. Weniger, Phys. Rev. D **91**, no. 6, 063003 (2015) [arXiv:1411.4647 [hep-ph]].
- [76] U. Ellwanger, J. F. Gunion and C. Hugonie, JHEP **0502**, 066 (2005) [hep-ph/0406215]. U. Ellwanger and C. Hugonie, Comput. Phys. Commun. **175**, 290 (2006) [hep-ph/0508022]. G. Belanger, F. Boudjema, C. Hugonie, A. Pukhov and A. Semenov, JCAP **0509**, 001 (2005) [hep-ph/0505142]. U. Ellwanger and C. Hugonie, Comput. Phys. Commun. **177**, 399 (2007) [hep-ph/0612134]. M. Muhlleitner, A. Djouadi and Y. Mambrini, Comput. Phys. Commun. **168**, 46 (2005) [hep-ph/0311167]. D. Das, U. Ellwanger and A. M. Teixeira, Comput. Phys. Commun. **183**, 774 (2012) [arXiv:1106.5633 [hep-ph]].
- [77] J. Huang, T. Liu, L. T. Wang and F. Yu, Phys. Rev. Lett. **112**, no. 22, 221803 (2014) [arXiv:1309.6633 [hep-ph]].
- [78] A. Butter, T. Plehn, M. Rauch, D. Zerwas, S. Henrot-Versill and R. Lafaye, arXiv:1507.02288 [hep-ph].